Nickel(II) and Zinc(II) *meso*-Tetracyclohexylporphyrins. Structural and Electronic Effects Induced by *meso*-Cyclohexyl Substitution in Metalloporphyrins†

Marc Veyrat,‡ René Ramasseul,‡ Ilona Turowska-Tyrk,§ W. Robert Scheidt,*,§ Marie Autret,|| Karl M. Kadish,*,|| and Jean-Claude Marchon*,‡

Laboratoire de Chimie de Coordination (URA CNRS 1194), Service de Chimie Inorganique et Biologique, Département de Recherche Fondamentale sur la Matière Condensée, CEA-Grenoble, 38054 Grenoble, France, Department of Chemistry and Biochemistry, University of Notre Dame, Notre Dame, Indiana 46556, and Department of Chemistry, University of Houston, Houston, Texas 77004

Received October 20, 1998

The synthesis and X-ray structures of the zinc(II) and nickel(II) complexes of *meso*-tetracyclohexylporphyrin H_2(TCHP) are described. The nonplanarity of the *meso* substituents results in steric crowding at the porphyrin periphery. In the solid state, the nickel(II) complex Ni(TCHP) has a ruffled porphyrin conformation while Zn(TCHP) exhibits a stepped distortion of the macrocycle. In chloroform solution, fast rotation of the cyclohexyl groups on the NMR time scale is observed at room temperature for both complexes. Temperature-dependent ^{1}H NMR spectra showed that the (−*g*,*g*,−*g*,*g*) conformer of Zn(TCHP) and Ni(TCHP) is prevalent in solution at low temperatures and gave an estimate for the rotation barrier of the cyclohexyl groups ($\Delta G_c^{\ddagger} = 10-12$ kcal mol^{-1}). In both complexes, the porphyrin ring is easier to oxidize and harder to reduce than in their tetraphenylporphyrin M(TPP) congeners, in agreement with the stronger electron-donating effect of the cyclohexyl group. The magnitude of the potential shift is larger for the first oxidation than for the first reduction, reflecting a smaller HOMO−LUMO energy gap and a greater degree of macrocycle distortion than in the M(TPP) derivatives. This information is of importance to understanding the protein regulation of electron-transfer processes by cytochrome c and other redox active proteins. Crystal data: Ni(TCHP)·$CHCl_3$·CH_3CN, monoclinic, *C*2/*c*, $a = 27.405(12)$, $b = 10.004(21)$, $c = 32.877(24)$ Å, $\beta = 107.71(3)°$ at 127 K, $Z = 8$. Zn(TCHP), monoclinic, $P2_1/a$, $a = 11.159(15)$, $b = 11.992(7)$, $c = 13.465(20)$ Å, $\beta = 102.85(16)°$ at 127 K, $Z = 2$.

Introduction

In the large family of meso-substituted porphyrins, 5,10,15,-20-tetracyclohexylporphyrin H_2(TCHP) is a recent addition[1] which can be viewed as a tetraphenylporphyrin derivative with fully hydrogenated *meso*-substituents. This macrocyclic ligand possesses some unusual steric and electronic features which have attracted recent interest. The nonplanarity of its bulky *meso*-cyclohexyl substituents has a strong influence on the stereochemistry of the porphyrin core in its metal complexes,[2,3] and their aliphatic nature has been shown to stabilize the less common $(d_{xz}d_{yz})^4(d_{xy})^1$ spin state in its low-spin ferric complexes.[4] In this paper we report in detail the synthesis of H_2(TCHP) **1** and the X-ray structures of its nickel(II) and zinc(II) complexes **2** and **3**; some of these results have been published in a preliminary communication.[2] We also describe the dynamic stereochemistry of the two complexes in chloroform solution, as well as their electrochemistry in dichloromethane and benzonitrile.

Experimental Section

Materials. Solvents and chemicals used for synthesis were obtained from Aldrich and used as received. Tetracyclohexylporphyrin was prepared according to a local modification of a literature procedure (vide infra).[1] Tetra-*n*-butylammonium perchlorate (TBAP) was purchased from Sigma, recrystallized from ethyl alcohol, and dried under vacuum at 40 °C for at least one week prior to use. Absolute dichloromethane dried over molecular sieves, obtained from Fluka, was used for electrochemical studies without further purification. Benzonitrile (PhCN) was purchased from Aldrich and distilled over P_2O_5 under vacuum prior to use.

H_2(TCHP). In a 5-L three-neck round-bottom flask was poured 4 L of dichloromethane containing 0.1% ethanol (*Note*: the presence of ethanol in the solvent dichloromethane is essential; no tetracyclohexylporphyrin was obtained if the solvent was ethanol-free, or if boron trifluoride was used as a catalyst instead of trifluoroacetic acid). Argon was bubbled for 45 min, and 4.50 g of cyclohexanecarboxaldehyde (40.1 mmol) was added, followed by 2.69 g of pyrrole (40.1 mmol). The mixture was stirred for 5 min, and a solution of 4.57 g of trifluoroacetic acid (40.1 mmol) in 10 mL of dichloromethane was added dropwise. The mixture was stirred for 5 h, 6.83 g of 2,3-dichloro-5,6-dicyanobenzoquinone (30.1 mmol) was added, and the solution was brought to reflux for 1.5 h. After cooling, the solvent volume was reduced to about 2.5 L, and the mixture was filtered on neutral alumina (activity I). To the filtrate was added 20 g of silica gel, and the solvent was evaporated to dryness. The resulting solid was placed on top of a column containing 250 g of silica gel, and the product was eluted with

† Abbreviations: TCHP = dianion of tetracyclohexylporphyrin; TPP = dianion of tetraphenylporphyrin; TBAP = tetra-*n*-butylammonium perchlorate; PhCN = benzonitrile.

‡ CEA-Grenoble.

§ University of Notre Dame.

|| University of Houston.

(1) Onaka, M.; Shinoda, T.; Izumi, Y.; Nolen, E. *Chem. Lett*. **1993**, 117.
(2) Veyrat, M.; Ramasseul, R.; Marchon, J. C.; Turowska-Tyrk, I.; Scheidt, W. R. *New J. Chem.* **1995**, *19*, 1199.
(3) Jentzen, W.; Hobbs, J. D.; Song, X.; Simpson, M. C.; Ema, T.; Nelson, N. Y.; Medforth, C. J.; Smith, K. M.; Veyrat, M.; Mazzanti, M.; Ramasseul, R.; Marchon, J. C.; Takeuchi, T.; Goddard, W. A., III; Shelnutt, J. A. *J. Am. Chem. Soc.* **1995**, *117*, 11085.
(4) Wolowiec, S.; Latos-Grazynski, L.; Toronto, D.; Marchon, J. C. *Inorg. Chem.* **1998**, *37*, 724. Erratum. *Ibid*. **1998**, *37*, 2096.

10.1021/ic981233i CCC: $18.00
Published on Web 03/31/1999

hexane/dichloromethane mixtures of increasing polarities (90/10, 85/15, and finally 65/35). The various pure fractions were combined, and the free base porphyrin was recrystallized from a dichloromethane−acetonitrile mixture. Yield: 1.49 g of tetracyclohexylporphyrin, **1**, (23%): MS−FAB+ *m*/*z* 639, MH^+; UV−vis (CH_2Cl_2) λ_{max}/nm 422, 525, 562, 603, 660; ^{1}H NMR, 200 MHz, $CDCl_3$, 20 °C, δ −1.60 (s, 2H, N−H), 1.83 (m, 12H, H_{4a}, H_{3a}), 2.14 (m, 12H, H_{4e}, H_{3e}), 2.58 (m, 8H, H_{2e}), 2.96 (m, 8H, H_{2a}), 4.76 (tt, 4H, H_1, J 12.5 Hz, J' 3.5 Hz), 9.46 (s, 8H, H_β); ^{13}C NMR, 75 MHz, $CDCl_3$, 20 °C, δ 26.7 (C_4), 28.5 (C_3), 38.7 (C_2), 46.9 (C_1), 122.5 (C_{meso}), 129.1(C_β), 143.7 (C_α).

Ni(TCHP). A 100 mg amount of **1** (0.16 mmol) and 390 mg of nickel acetate (1.6 mmol) were dissolved in 20 mL of a 1/1 chloroform/ethanol mixture. The resulting solution was brought to reflux for 1 h, and then evaporated to dryness. The solid product was purified by column chromatography on silica gel (50 g) using a 1/1 dichloromethane/cyclohexane mixture as eluent, and recrystallized from chloroform−acetonitrile. Yield: 100 mg of nickel(II) tetracyclohexylporphyrin, **2**, (90%): MS−FAB+ *m*/*z* 694, M^+; UV−vis (CH_2Cl_2): λ_{max}/nm 425, 508, 550, 586; ^{1}H NMR, 200 MHz, $CDCl_3$, 20 °C, δ: 1.70 (m, 12H, H_{4a}, H_{3a}), 2.09 (m, 12H, H_{4e}, H_{3e}), 2.42 (m, 8H, H_{2e}), 2.73 (m, 8H, H_{2a}), 4.21 (tt, 4H, H_1, J 12.5 Hz, J' 3.4 Hz), 9.21 (s, 8H, H_β); ^{13}C NMR, 75 MHz, $CDCl_3$, 20 °C, δ: 26.6 (C_4), 28.2 (C_3), 38.1 (C_2), 45.6 (C_1), 121.2 (C_{meso}), 130.6 (C_β), 139.1 (C_α).

Zn(TCHP). This complex was prepared from **1** and zinc acetate by a procedure entirely similar to that used for Ni(TCHP). Yield: 95 mg (85%) of zinc(II) tetracyclohexylporphyrin, **3**, after recrystallization from chloroform-pentane: MS−FAB+ *m*/*z* 700, M^+; UV−vis (CH_2Cl_2) λ_{max}/nm 423, 524, 562, 624; ^{1}H NMR, 200 MHz, $CDCl_3$, 20 °C, δ 1.90 (m, 12H, H_{4a}, H_{3a}), 2.17 (m, 12H, H_{4e}, H_{3e}), 2.62 (m, 8H, H_{2e}), 3.10 (m, 8H, H_{2a}), 5.06 (tt, 4H, H_1, J 12.5 Hz, J' 3.5 Hz), 9.75 (s, 8H, H_β); ^{13}C NMR, 75 MHz, $CDCl_3$, 20 °C, δ 26.8 (C_4), 28.7 (C_3), 38.8 (C_2), 47.2 (C_1), 124.1 (C_{meso}), 129.6 (C_β), 143.7 (C_α).

X-ray Structure Determinations of Ni(TCHP) and Zn(TCHP). Red, single crystals suitable for X-ray structure determinations were obtained by recrystallization from chloroform−acetonitrile. Unit cell parameter determination with an area detector have been described earlier.[5] Data collection was processed with an Enraf-Nonius FAST area detector diffractometer with a FR-588 low-temperature device and graphite-monochromated Mo Kα radiation. For **2**, a total of 9857 collected reflections were considered as observed ($F_o \geq 1.9\sigma(F_o)$), of which 3726 were unique; for **3**: 7701 and 2799 ($F_o \geq 1.7\sigma(F_o)$), respectively. Intensities of all reflections were reduced using Lorentz and polarization corrections. Both structures were solved by Patterson methods from the SHELXS86 program.[6] For **2**, the position of Ni was used in the DIRDIF program that enabled us to find all atoms. For **3**, positions of all atoms were revealed. For all nonhydrogen atoms, anisotropic least-squares refinement was used. Hydrogen atoms were included as fixed, idealized contributions. The refinement converged to a value of $R = 0.092$, $wR = 0.103$ and $R = 0.072$, $wR = 0.087$ for **2** and **3**, respectively. The maximum electron density on a final difference Fourier map was 1.02 e/Å^3 (in a distance 2.30 Å from C(3)) and the minimum was −0.65 e/Å^3 for **2** and 1.05 e/Å^3 (1.35 Å from N(2)) and −0.80 e/Å^3 for **3**, respectively. Other programs used in this study included local modifications of Beurskens, Bosman, Doesburg, Gould, van den Hark, Prick, Noordik, Parthasarathi, Bruins, Slot, Haltiwanger, Strumpel, and Smits's DIRDIF, Busing and Levy's ORFFE and ORFLS, Jacobson's ALLS, Zalkin's FORDAP, and Johnson's ORTEP2. Atomic form factors were from Cromer and Mann.[7] Real and imaginary corrections for anomalous dispersion in the form factor of the Ni and Zn atoms were from Cromer and Liberman.[8] Scattering factors for hydrogen were from Stewart et al.[9]

Instrumentation. UV−vis spectra were recorded on a Perkin-Elmer Lambda 9. ^{1}H NMR spectra were recorded on a Bruker 200 or 300 MHz NMR spectrometer. Chemical shifts are referenced to tetramethylsilane. Cyclic voltammetry was carried out with an EG&G Model 173 potentiostat or an IBM Model EC 225 Voltammetric Analyzer. Current−voltage curves were recorded on an EG&G Princeton Applied Research Model RE-0151 X-Y recorder. A three-electrode system was used and consisted of a glassy carbon or platinum button working electrode, a platinum wire counter electrode, and a saturated calomel reference electrode (SCE). This reference electrode was separated from the bulk of the solution by a fritted-glass bridge filled with the solvent/supporting electrolyte mixture. Ferrocene was used as an internal standard, but all potentials are referenced to the SCE. UV−visible spectroelectrochemical experiments were performed with a home-built platinum thin-layer electrode of the type described in the literature.[10] Potentials were applied and monitored with an EG&G Model 173 potentiostat. Time-resolved UV−visible spectra were recorded with a Princeton Instrument PDA-1024 diode array and ST 1000 detector controller. Data acquisition and processing were performed using OSMA and PSMA software.

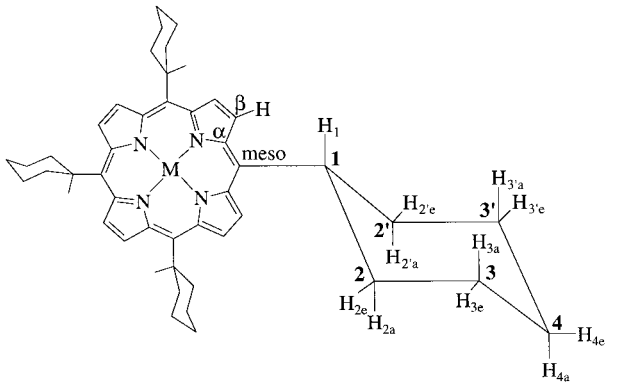

Figure 1. A schematic view of the (−*g*,*g*,−*g*,*g*) conformer of a M(II)−tetracyclohexylporphyrin complex. One cyclohexyl group has been artificially enlarged for better visibility of the stereochemistry and of the atom labels.

Results

Synthesis and Spectral Characterization. We find that **1** can be obtained in 23% yield by conventional Lindsey condensation[11] of pyrrole and cyclohexanecarboxaldehyde in dichloromethane containing 0.1% ethanol, using trifluoroacetic acid as the catalyst. As explained below for **2** and **3**, the highly symmetric ^{1}H and ^{13}C NMR spectra of **1** are consistent with fast averaging of equatorially bound cyclohexyl groups in a chair conformation shown schematically in Figure 1.

X-ray Structures. A summary of crystallographic data is shown in Table 1. The structures of **2** and **3**, which are shown, respectively, in Figures 2 and 3, confirm the equatorial bonding of the *meso*-cyclohexyl groups, consistent with the greater stability of equatorially substituted cyclohexane isomers.[12] Conformations in which the mean plane of the cyclohexyl groups would be coplanar with that of the porphyrin obviously are restricted by steric crowding between H_{2e} and H_β. In the observed geometry, these planes are approximately orthogonal, resulting in gauche conformations ($\pm g$, see below) of the $C_\alpha-C_{meso}-C_1-C_2$ fragments. Bumping interactions between hydrogen atoms in axial position on C_1 and on the neighboring β-pyrrolic position are effectively relieved by minute rotations of the cyclohexyl groups off the strictly orthogonal orientation. A relative g or $-g$ conformation can be defined for each of the four cyclohexyl substituents,[13] depending on the clockwise or

(5) Scheidt, W. R.; Turowska-Tyrk, I. *Inorg. Chem*. **1994**, *33*, 1314.
(6) Sheldrick, G. M. *Acta Crystallogr., Sect. A* **1990**, *46*, 467.
(7) Cromer, D. T.; Mann, J. B. *Acta Crystallogr., Sect. A* **1968**, *24*, 321.
(8) Cromer, D. T.; Liberman, D. J. *J. Chem. Phys*. **1970**, *53*, 1891.
(9) Stewart, R. F.; Davidson, E. R.; Simpson, W. T. *J. Chem. Phys*. **1965**, *42*, 3175.
(10) Lin, X. Q.; Kadish, K. M. *Anal. Chem.* **1985**, *57*, 1498.
(11) Lindsey, J. S.; Wagner, R. W. *J. Org. Chem*. **1989**, *54*, 828.
(12) Eliel, E. L.; Wilen, S. H.; Mander, L. N. *Stereochemistry of Organic Compounds*; Wiley: New York, 1994; Chapter 11, p 694.

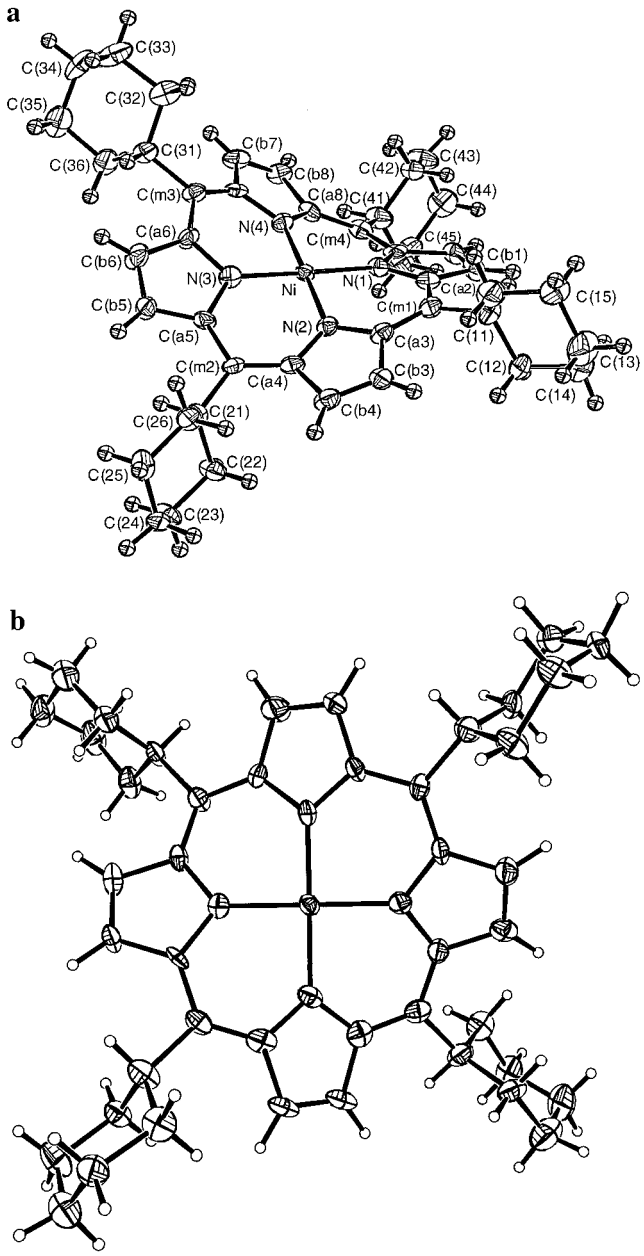

Figure 2. (a) The structure of Ni(TCHP) **2** in the crystal, showing the ruffled distortion of the porphyrin. Thermal ellipsoids of the H atoms are reduced for clarity. Selected bond lengths (Å) and angles (deg): Ni−N(1) 1.892(8), Ni−N(2) 1.897(9), Ni−N(3) 1.882(9), Ni−N(4) 1.881(9), N(1)−Ni−N(2) 90.7(4), N(1)−Ni−N(3) 178.9(4), N(1)−Ni−N(4) 89.7(4), N(2)−Ni−N(3) 89.9(4), N(2)−Ni−N(4) 178.1(4), N(3)−Ni−N(4) 89.7(4). (b) Top view showing the (−*g*,*g*,*g*,*g*) conformation of the cyclohexyl groups.

anticlockwise orientation of the C_1-H_1 vector around the porphyrin ring. Thus, four conformers can be expected for a metal(II)−tetracyclohexylporphyrin complex, i.e. (*g*,*g*,*g*,*g*), (−*g*,*g*,*g*,*g*), (−*g*,−*g*,*g*,*g*), and (−*g*,*g*,−*g*,*g*)—or the equivalent descriptors obtained by permutation of *g* for −*g* (Figure 4). The unique solid state conformation found for Ni(TCHP) **2** is (−*g*,*g*,*g*,*g*), while that for Zn(TCHP) **3** is (−*g*,*g*,−*g*,*g*).

The porphyrin ring of **2** has a strongly ruffled conformation[14] as in many other nickel porphyrin complexes. In **2**, this ruffling

(13) (a) Colombus, I.; Biali, S. *J. Org. Chem.* **1993**, *58*, 7029. (b) Colombus, I.; Biali, S. *J. Org. Chem.* **1994**, *59*, 3402. (c) Colombus, I.; Cohen, S.; Biali, S. *J. Am. Chem. Soc.* **1994**, *116*, 10306. (d) Colombus, I.; Biali, S. *J. Org. Chem.* **1994**, *59*, 8132.

(14) Scheidt, W. R.; Lee, Y. J. *Struct. Bond. (Berlin)* **1987**, *64*, 1.

Table 1. Crystallographic Data for Ni(TCHP) and Zn(TCHP)

	Ni(TCHP)·$CHCl_3$·CH_3CN	Zn(TCHP)
formula	$C_{44}H_{52}N_4Ni$·$CHCl_3$·CH_3CN	$C_{44}H_{52}N_4Zn$
FW	856.04	702.31
crystal system	monoclinic	monoclinic
a, Å	27.405(12)	11.159(15)
b, Å	10.004(21)	11.992(7)
c, Å	32.877(24)	13.465(20)
β, deg	107.71(3)	102.85(16)
V, Å^3	8586(30)	1757(7)
space group	*C*2/*c*	$P2_1/a$
Z	8	2
D_c, g/cm^3	1.318	1.322
radiation, Å	0.71073	0.71073
μ, mm^{-1}	0.676	0.748
temperature, °C	−146(1)	−146(1)
R1[a]	0.092	0.072
wR2	0.103	0.087

[a] $R1 = \sum||F_o| - |F_c||/\sum|F_o|$ and $wR2 = \{\sum[w(F_o^2 - F_c^2)^2]/\sum[wF_o^4]\}^{1/2}$. The conventional *R*-factors R1 are based on *F*, with *F* set to zero for negative F^2. The criterion of $F^2 < 2\sigma(F^2)$ was used only for calculating R1. *R*-factors based on F^2 (wR2) are statistically about twice as large as those based on *F*, and *R*-factors based on all data will be even larger.

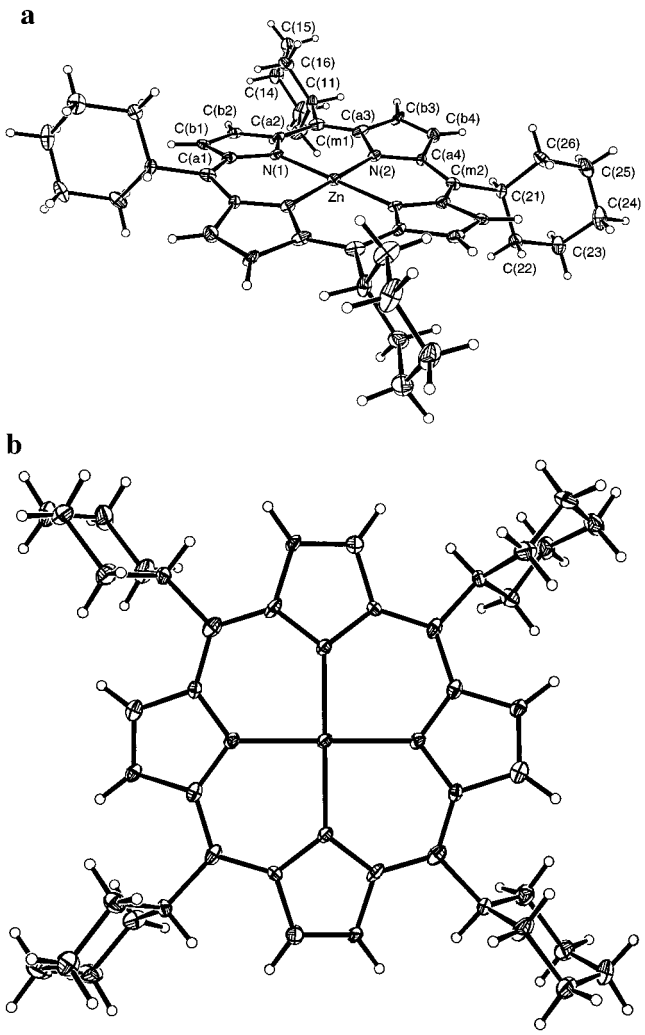

Figure 3. (a) The structure of Zn(TCHP) **3** in the crystal, showing the step-shaped distortion of the porphyrin. Selected bond lengths (Å) and angles (deg): Zn−N(1) 2.040(5), Zn−N(2) 2.018(5), N(1)−Zn−N(2) 90.24(21), N(2)−Zn−N(1) 89.76(21). (b) Top view showing the (−*g*,*g*,−*g*,*g*) conformation of the cyclohexyl groups.

results from the small size of the nickel(II) ion concurrent with steric crowding at the macrocycle periphery,[3] and it leads to

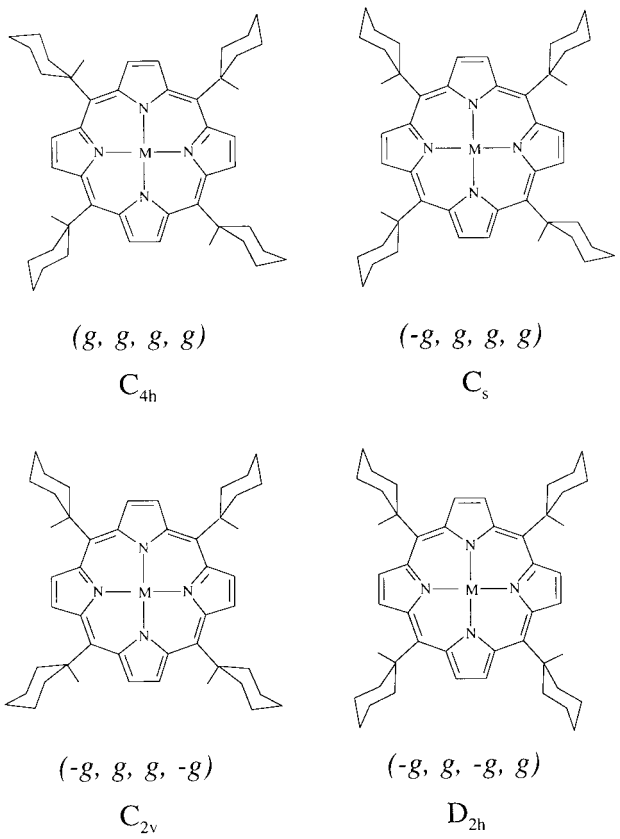

Figure 4. The four possible conformers of a M(II)−tetracyclohexylporphyrin complex.

the shortest values observed for the nickel−porphyrin nitrogen distances (Ni−N_{Pav} = 1.888(9) Å). The combination of a (−*g*,*g*,*g*,*g*) conformation and of a ruffled distortion in **2** results in a chiral Ni(TCHP) molecule; both enantiomers are present in the crystal lattice since the space group is nonchiral.

The porphyrin core conformation in **3** is also decidedly nonplanar. The Zn atom sits on a crystallographically required inversion center, and the porphyrin core has an approximate C_{2h} symmetry; it exhibits a step-shaped distortion[14] in which two neighboring pyrrole rings are tilted below the mean N_4 plane while the other two are tilted above. This type of nonplanar distortion has been found in a number of complexes that have a metal at the center of the ring,[15] as well as in some out-of-plane complexes.[16] The two conformations reflect the nonplanarity required by the peripheral substituents[17] and the differing size of the two metal ions.

Dynamic NMR Spectroscopy. The ^{1}H and ^{13}C NMR spectra of **2** were assigned using a combination of 2D ^{1}H−^{1}H and ^{13}C−^{1}H correlation.[2] At room temperature a single peak is observed in the ^{13}C and ^{1}H spectra for the resonances of positions 2 and 2′, and for those of positions 3 and 3′ of the cyclohexyl groups, and for the pyrrole β position as well. The resonance of H_1 is a triplet of a triplet, and the values of the two coupling constants are in the range expected for axial−axial (J = 12.5 Hz) and axial−equatorial (J' = 3.4 Hz) interactions,[12] in agreement with the equatorial bonding of the cyclohexyl substituents. Very similar ^{1}H and ^{13}C spectra were obtained for **3** at room temperature.

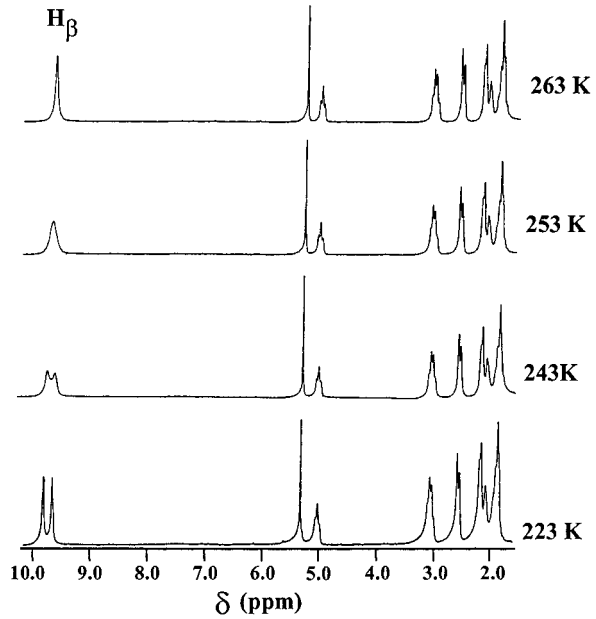

Figure 5. Temperature-dependent 300 MHz ^{1}H NMR spectra of Zn(TCHP) in CD_2Cl_2.

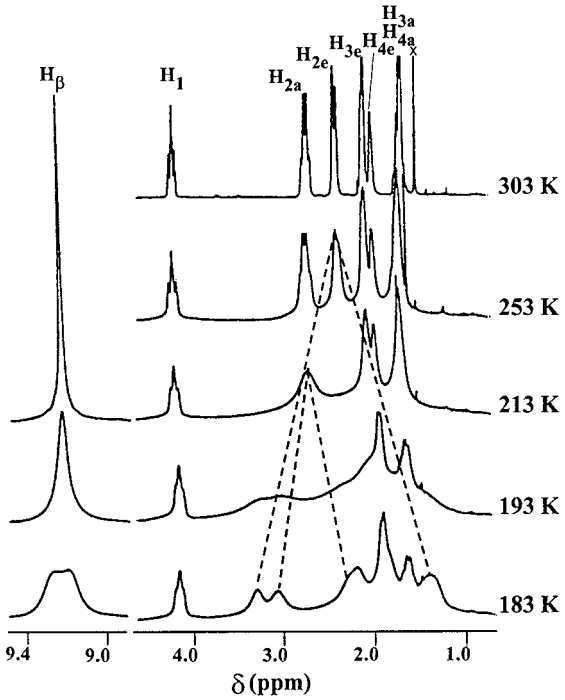

Figure 6. Temperature-dependent 300 MHz ^{1}H NMR spectra of Ni(TCHP) in CD_2Cl_2.

Upon lowering the temperature, the ^{1}H NMR spectrum of **3** shows no change in the cyclohexyl resonances, while the peak of the pyrrolic protons broadens and splits in a pair of equivalent signals below 250 K (Figure 5).

The temperature dependence of the ^{1}H NMR spectrum of **2** is more complex (Figure 6), and the underlying conformational changes are not immediately apparent (vide infra). At 183 K, the lowest temperature which could be attained in these experiments, the resonance of the pyrrole protons begins to split into two lines. The resonance of H_1 remains unchanged throughout the temperature range from 303 to 183 K, while

(15) See, for example: (a) Kutzler, F. W.; Swepston, P. N.; Berkovitch-Yellin, Z.; Ellis, D. E.; Ibers, J. A. *J. Am. Chem. Soc.* **1983**, *105*, 2996. (b) Jia, S. L.; Jentzen, W.; Shang, M.; Song, X. Z.; Ma, J. G.; Scheidt, W. R.; Shelnutt, J. A. *Inorg. Chem.* **1998**, *37*, 4402.

(16) See, for example: Belcher, W. J.; Boyd, P. D. W.; Brothers, P. J.; Liddell, M. J.; Rickard, C. E. F. *J. Am. Chem. Soc.* **1994**, *116*, 8416.

(17) Shelnutt, J. A.; Song, X. Z.; Ma, J. G.; Jia, S. L.; Jentzen, W.; Medforth, C. J. *Chem. Soc. Rev.* **1998**, *27*, 31.

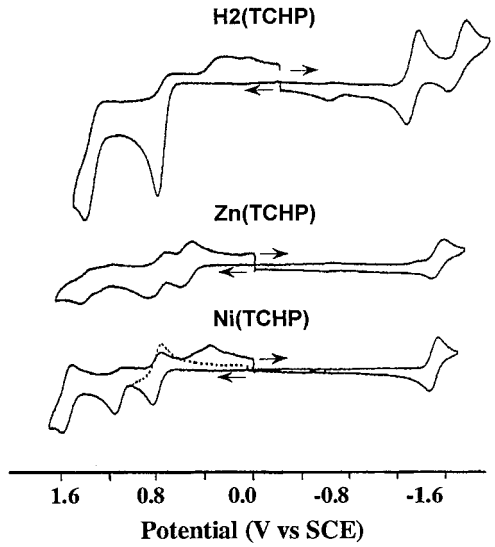

Figure 7. Cyclic voltammograms of tetracyclohexylporphyrin derivatives in dichloromethane containing 0.1 M TBAP.

Table 2. Half Wave Potentials (V vs SCE) for Oxidation and Reduction of TCHP Derivatives in CH_2Cl_2, Containing 0.1 M TBAP

		potentials					
		oxidation				reduction	
compound	solvent						
H_2(TCHP)	CH_2Cl_2			+1.44[a]	+0.83[a]	−1.30	−1.67
Zn(TCHP)	CH_2Cl_2	+1.41	+1.25	+0.80	+0.57	−1.52	
Ni(TCHP)	CH_2Cl_2		+1.56	+1.17[a]	+0.81	−1.49	

[a] Value given is E_{pa}, at 100 mV/s.

those of H_{2a} and H_{2e} show extensive broadening and splitting. Broadening of the peaks of H_{3a} and H_{3e} is observed below 193 K.

Electrochemistry. The cyclic voltammograms of the tetracyclohexylporphyrin free base and of its nickel and zinc complexes in CH_2Cl_2 containing 0.1 M TBAP are presented in Figure 7, and the redox potentials are summarized in Table 2.

H_2(TCHP). Two reductions are observed in CH_2Cl_2. The first, at $E_{1/2} = -1.30$ V, is reversible. The second, at $E_{1/2} = -1.67$ V, is not completely reversible and gives rise to a new reoxidation peak at $E_{pa} = -0.61$ V. Two oxidations are also seen. The first, at $E_{1/2} = +0.83$ V, is not completely reversible and give rise to a new rereduction peak at $E_{pc} = +0.06$ V. This irreversible process is probably due to the formation of an isoporphyrin. The intensity of this wave increases when holding the potential after the first oxidation. A second irreversible wave, at $E_{pa} = +1.44$ V, is also observed.

In the case of H_2(TPP), four reversible redox processes are observed.[18] Comparing the data of H_2(TCHP) with that of H_2(TPP) indicates that the processes are all shifted toward negative potentials for the TCHP derivative. The difference is 100 and 120 mV for the two reductions and 190 mV for the first oxidation of H_2(TCHP) in CH_2Cl_2.

Zn(TCHP). Only one reduction is observed at $E_{1/2} = -1.52$ V in CH_2Cl_2. Four oxidation processes are observed. The first at $E_{1/2} = +0.57$ V is quasireversible ($|E_{pa} - E_{pc}| = 120$ mV) and so is the second which is located at $E_{1/2} = +0.8$ V ($|E_{pa} - E_{pc}| = 120$ mV). The last two processes have a smaller current and are located at $E_{1/2} = +1.25$ V and $E_{1/2} = +1.41$ V.

Zn(TPP) and other zinc porphyrins have been extensively studied.[19] All of the previously studied complexes show two reductions leading to a π-anion radical and dianion. A π-cation radical and the dication are also formed during the oxidation. Unexpectedly, four oxidation steps are seen in the case of Zn(TCHP) but one, in addition to the two expected, may be due to isoporphyrin formation. In benzonitrile, the cyclic voltammogram shows three oxidations which are at potentials close to those measured in CH_2Cl_2. Only the first two are completely reversible. Compared to Zn(TPP), the first oxidation and reduction potentials of Zn(TCHP) are shifted toward negative values, by 210 mV for the first process and by 140 mV for the last one.

Ni(TCHP). A single reversible reduction is measured in CH_2Cl_2 at $E_{1/2} = -1.49$ V when scanning the potentials toward cathodic values. However, three oxidations are observed. The first, at $E_{1/2} = +0.81$ V, is reversible. The second, at $E_{pa} = +1.17$ V, is coupled with a rereduction peak at $E_{pc} = +0.35$ V and likely gives an isoporphyrin. The third oxidation, at $E_{1/2} = +1.56$ V, is not completely reversible. The cyclic voltammogram in benzonitrile shows three oxidations waves, but the ratios i_{pa}/i_{pc} is higher than 1.0, suggesting an EC mechanism.

A number of nickel porphyrins shows two one-electron reductions, the first of which leads to a π-anion radical.[19] The separation between the two reduction waves is 440 mV in the case of Ni(TCHP). This may be compared to a 420 ± 50 mV separation generally observed for porphyrins which undergo electron addition at the conjugated π-ring system to give porphyrin π-anion radicals. In the case of Ni(TPP) the first oxidation and the first reduction are ring centered, but the electron-transfer site can be shifted toward the metal by changing different factors such as the temperature or the solvent.[20]

By comparing the measured redox potentials of Ni(TCHP) with those of Ni(TPP), it appears that the values of the former complex are shifted toward negative potentials. The potential difference is 210 mV for the first reduction and 240 mV for the first oxidation, in CH_2Cl_2.

Spectroelectrochemistry. Zn(TCHP). In thin-layer time scale, the voltammogram of the zinc compound shows only two reversible oxidations in PhCN, 0.2 M TBAP. The third oxidation and the reduction previously observed by cyclic voltammetry are not reversible in these experimental conditions. The UV−visible spectra recorded during thin-layer controlled-potential oxidations are presented in Figure 8, and the data are summarized in Table 3. The electronic absorption spectrum of Zn(TCHP) shows one Soret band, at $\lambda = 422$ nm, and two visible bands located at $\lambda = 559$ and 602 nm.

During the first oxidation, when the controlled-potential is set to +0.7 V, the Soret intensity decreases, but no significant shift is observed ($\lambda = 420$ nm for the oxidized compound). In the same time, the visible bands decrease and widen, and a weak broad absorption band is then observed in this region. These spectral modifications are reversible when the controlled potential is set back to 0.0 V.

The spectral changes observed upon the second controlled-potential oxidation, at +0.95 V, indicate that the Soret band dramatically decreases and broadens in the same time (Figure 8). No visible band is seen in the spectrum of the doubly oxidized species, $[Zn(TCHP)]^{2+}$. Contrary to what was observed during the first oxidation, the UV−visible spectral modifications are not reversible, and the spectrum of the singly oxidized form cannot be recovered when the potential is set back to +0.7 V.

(18) Davis, D. G. *Porphyrins*; Dolphin, D., Ed.; Academic: New York, 1978; Vol. 5 (Part C), p 127.

(19) Kadish, K. M.; Davis, D. G. *Ann. N.Y. Acad. Sci.* **1973**, *206*, 495.

(20) Kadish, K. M. *Progr. Inorg. Chem.* **1986**, *34*, 435.

Table 3. Spectral Data for Ni(TCHP) and Zn(TCHP) and Their Reduction and Oxidation Products, in PhCN Containing 0.2 M TBAP

			λ_{max} (nm) (absorption)[a]	
compound	reaction	E_{appl} (V)	Soret	visible
Zn(TCHP)	neutral	none	422 (1.00)	559 (0.08), 602 (0.06)
	1st oxidation	+0.70	420 (0.56)	
	2nd oxidation	+0.95	420 (0.21)	
Ni(TCHP)	neutral	none	422 (1.00)	546 (0.11), 585 (0.03)
	1st oxidation	+1.00	422 (0.71)	
	2nd oxidation	+1.25	428 (0.28)	
	1st reduction	−1.60	424 (0.60), 451 (sh)	552 (0.06), 604 (0.04)

[a] Arbitrary units.

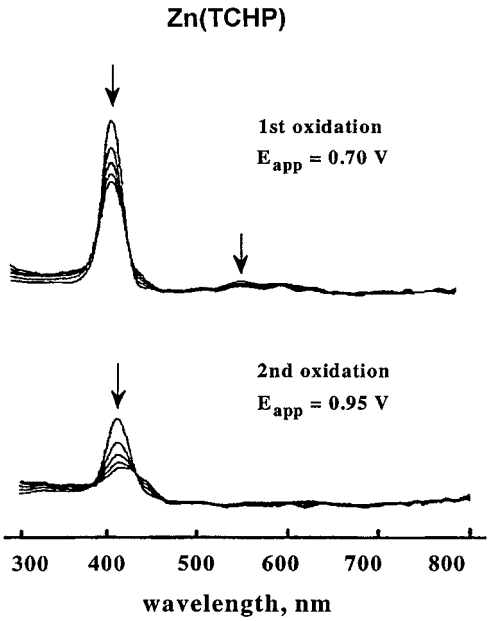

Figure 8. UV−visible spectral changes obtained during the controlled-potential oxidations of Zn(TCHP) in benzonitrile containing 0.2 M TBAP.

Ni(TCHP). Three processes, the reduction and the first two oxidations, were studied by thin-layer spectroelectrochemistry, although the second oxidation is not completely reversible. The UV−visible spectra obtained are presented in Figure 9. The electronic absorption spectrum of the neutral species shows a Soret band located at $\lambda = 422$ nm, and two bands at 546 and 585 nm in the visible region.

During the controlled-potential reduction at −1.60 V, the Soret band decreases in intensity. No significant shift is observed ($\lambda = 424$ nm for the reduced species), but a shoulder at $\lambda = 451$ nm rises. In the visible region, the initial band at 546 nm decreases and slightly shifts to 552 nm. A weak band at 604 nm is also present in the spectrum of the singly reduced species. The changes are reversible and the initial spectrum is totally recovered by applying the controlled potential back to 0.0 V after the electroreduction.

Upon the controlled potential oxidation at +1.00 V, the Soret band decreases without shifting, and the initial visible band is replaced by two less intense absorption bands at 551 and 605 nm. Comparatively to the controlled-potential reduction, these spectral changes are fully reversible.

During the oxidation of $[Ni(TCHP)]^+$, a large decrease and a small red shift (from 421 to 428 nm) of the Soret band are observed (Figure 9). In the spectrum of the double-oxidized species, no absorption bands are seen in the visible region. The spectral changes observed during this controlled-potential oxidation are not reversible, since the UV−visible spectrum of the singly oxidized form cannot be recovered.

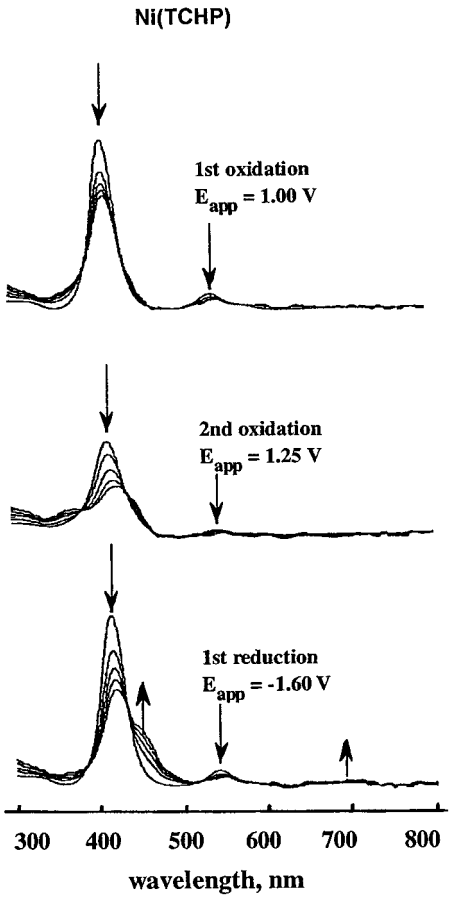

Figure 9. UV−visible spectral changes obtained during the controlled-potential oxidations and reduction of Ni(TCHP) in benzonitrile containing 0.2 M TBAP.

Similar UV−visible spectral modifications are observed for Ni(TCHP) and Zn(TCHP) during the first, as well as during the second, oxidation process. The fact that, in all cases, the Soret band strongly decreases but does not shift suggests that these oxidations are ring centered, leading for both compounds to the cation radical and dication species.

Moreover, for both compounds, the first two oxidations are separated by the same potential value, $\Delta E_{1/2} = 250$ mV. This corroborates the hypothesis that the same reactions occur during the oxidations of these two porphyrins. By comparison, the $E_{1/2}$ between two ring-centered oxidations, in the case of almost planar porphyrins, is generally around 400 mV.

Discussion

Dynamic Stereochemistry in Solution. Zn(TCHP). The high symmetry observed at room temperature in the ^{13}C and ^{1}H spectra of **3** imply fast rotation of the cyclohexyl substituents. The splitting of the pyrrole proton resonance below 250 K is

consistent with a slower cyclohexyl exchange on the NMR time scale. From the coalescence temperature $T_c = 250 \pm 5$ K and frequency difference $\Delta\nu = 45 \pm 1$ Hz at 223 K, the energy barrier $\Delta G_c^{\ddagger}$ for cyclohexyl group rotation was calculated by the Eyring equation: $\Delta G_c^{\ddagger} = 12 \pm 0.5$ kcal mol^{-1}. The fact that the pyrrole β-H peak splits into a pair of singlets indicates that, among the four possible conformers, only the ($-g,g,-g,g$) species with D_{2h} symmetry is present in solution at low temperatures. Since this species is also the only one found in the crystal structure, it appears that it has the lowest energy of the four conformers.

Ni(TCHP). Similarly, the observed symmetry of the ^{13}C and ^{1}H spectra of **2** at room temperature indicates that rotation of the cyclohexyl substituents is fast on the NMR time scale. Since the ruffled porphyrin which is observed in the crystal structure of **2** is probably also present in solution, inversion of the macrocycle is probably fast too.[21] Here again, the fact that the pyrrole peak splits into two lines below 183 K indicates that the ($-g,g,-g,g$) species is prevalent in solution at low temperatures; however, the ruffled distortion of this species has an important consequence. Inversion of a D_2-symmetric ruffled ($-g,g,-g,g$) species produces the D_2-symmetric enantiomorph which is undistinguishable by NMR. In the fast exchange regime, an average peak is obtained for each conformer of the inverting porphyrin, while in the slow exchange regime a single set of resonances is also observed since the two ruffled conformers are an enantiomeric pair. Thus, the energy barrier for porphyrin inversion cannot be obtained in this NMR experiment, and a single dynamic process, i.e., cyclohexyl group rotation, is responsible for the temperature-dependent changes in the spectra of **2**.

In addition to the splitting of the pyrrole proton peak, the resonances of H_{2a} and of H_{2e} exhibit a complex behavior as the solution of **2** is cooled to low temperatures. A tentative interpretation of these splittings is proposed in Figure 6. The peak of H_{2e} first broadens to the point of complete vanishing at 213 K, while at that temperature the peak of H_{2a} is broad but visible. At 183 K, each resonance is split into two peaks, indicating inequivalence of the two faces of the ruffled porphyrin in the slow exchange limit (see Figure 1). With the assumption that cyclohexyl group rotation is the common origin of the observed spectral changes for the three types of protons, the energy barrier $\Delta G_c^{\ddagger}$ for this process can be calculated for each type, with the following results: H_β ($\Delta\nu = 20 \pm 2$ Hz at 183 K): $\Delta G_c^{\ddagger} = 9.5 \pm 0.5$ kcal mol^{-1} at $T_c = 190 \pm 5$ K; H_{2a} ($\Delta\nu = 240 \pm 10$ Hz at 183 K): $\Delta G_c^{\ddagger} = 9.0 \pm 0.5$ kcal mol^{-1} at $T_c = 200 \pm 5$ K; H_{2e} ($\Delta\nu = 560 \pm 20$ Hz at 183 K): $\Delta G_c^{\ddagger} = 9.6 \pm 0.5$ kcal mol^{-1} at $T_c = 220 \pm 5$ K. The good agreement between the three calculated values of the energy barrier supports the starting hypothesis.

Thus, the rotation barrier of the cyclohexyl group is lower in the highly ruffled nickel complex (ca. 10 kcal mol^{-1}) than in the stepped zinc complex (ca. 12 kcal mol^{-1}). For comparison, rotation barriers of 15−20 kcal mol^{-1} are typically found for TPP complexes.[22] The lower rotation barriers found in this investigation (10−12 kcal mol^{-1}) for the more bulky *meso* substituents in TCHP complexes is probably related to their greater flexibility and to the higher degree of nonplanar distortion of their porphyrin cores.

Table 4. Half Wave Potentials (V vs SCE) and HOMO−LUMO Energy Gap (V) for TCHP and TPP Derivatives in CH_2Cl_2

compound	1st red.	ΔE(red.)[a]	1st ox.	ΔE(ox.)[a]	HOMO−LUMO gap
H_2(TCHP)	−1.30	−100	+0.83	−190	2.13
H_2(TPP)	−1.20		+1.02		2.22
Zn(TCHP)	−1.52	−140	+0.57	−210	2.09
Zn(TPP)	−1.38		+0.78		2.16
Ni(TCHP)	−1.49	−210	+0.81	−240	2.30
Ni(TPP)	−1.28		+1.05		2.33

[a] ΔE (mV) = [$E_{1/2}$(H_2(TCHP))] − [$E_{1/2}$(H_2(TPP))].

Electrochemistry. The redox potentials of the tetracyclohexylporphyrin complexes obtained by cyclic voltammetry in dichloromethane are summarized in Table 2. None of the investigated complexes are stable upon oxidation, and an isoporphyrin is probably formed in CH_2Cl_2 after the second oxidation of Ni(TCHP) and H_2(TCHP). Evidence for this assignment is given by the rereduction process observed at peak potentials between +0.6 V and +0.2 V on the reverse potential scan.

Thin-layer, time-dependent electronic absorption spectra were taken during the first two oxidations of Zn(TCHP) and Ni(TCHP) in PhCN containing 0.2 M TBAP (see Figures 8 and 9 and Table 3). Similar spectral changes are observed for both compounds. The intensity of the Soret band decreases upon the first oxidation while the visible bands are weak and ill-defined in the final spectra. Both of the doubly oxidized porphyrins have a very weak Soret band suggesting that porphyrin π-cation radicals followed by dications are obtained upon oxidation. The UV−visible changes obtained upon the thin-layer electroreduction of Ni(TCHP) indicate generation of a porphyrin π-anion radical species.

Table 4 summarizes potentials for the first reduction and first oxidation of the investigated TCHP derivatives and the corresponding TPP species. The introduction of cyclohexyl groups onto the *meso* positions of the porphyrin macrocycle leads to complexes which are easier to oxidize and harder to reduce than the corresponding tetraphenylporphyrins. The effect of electron-donating substituents onto the porphyrin ring is to raise the energy of both the HOMO and the LUMO, which results in an anodic potential shift when going from the TPP to the TCHP species. This is consistent with the electron-donating effect of the cyclohexyl groups as compared to the phenyl groups.

For each compound, the magnitude of the potential shift (see Table 4) is larger in the case of the first oxidation than in the case of the first reduction. This indicates that the HOMO is more affected by the introduction of the cyclohexyl groups than is the LUMO. The potential difference between the first oxidation and the first reduction, $E_{1/2}$(ox) − $E_{1/2}$(red), at the porphyrin macrocycle represents the electrochemical HOMO−LUMO energy gap. For the case of the free base porphyrin and the nickel and the zinc complexes investigated in the present study, the electrochemical HOMO−LUMO gap is slightly

(21) (a) Inversion of enantiomorphically ruffled conformers of nickel(II) *ccccc*-octaethylpyrrocorphinate with an inversion barrier $\Delta G_c^{\ddagger} = 11.3 \pm 0.1$ kcal mol^{-1} has been reported. See Waditschatka, R.; Kratky, C.; Jaun, B.; Heinzer, J.; Eschenmoser, A. *J. Chem. Soc., Chem. Commun.* **1985**, 1604. See also (b) Medforth, C. J.; Senge, M. O.; Smith, K. M.; Sparks, L. D.; Shelnutt, J. A. *J. Am. Chem. Soc.* **1992**, *114*, 9859. (c) Veyrat, M.; Maury, O.; Faverjon, F.; Over, D. E.; Ramasseul, R.; Marchon, J. C.; Turowska-Tyrk, I.; Scheidt, W. R. *Angew. Chem., Int. Ed. Engl.* **1994**, *33*, 220.

(22) (a) Bonnet, J. J.; Eaton, S. S.; Eaton, G. R.; Holm, R. H.; Ibers, J. A. *J. Am. Chem. Soc.* **1973**, *95*, 2141. (b) Fournari, P.; Guilard, R.; Fontesse, M.; Latour, J. M.; Marchon, J. C. *J. Organomet. Chem.* **1976**, *110*, 205. (c) Eaton, S. S.; Eaton, G. R. *J. Am. Chem. Soc.* **1977**, *99*, 6594. (d) Eaton, S. S.; Fishwild, D. M.; Eaton, G. R. *Inorg. Chem.* **1978**, *17*, 1542. (e) Laurie, A.; Shroyer, W.; Lorberau, C.; Eaton, S. S.; Eaton, G. R. *J. Org. Chem.* **1980**, *45*, 4296. See also: Noss, L.; Liddell, P. A.; Moore, A. L.; Moore, T. A.; Gust, D. *J. Phys. Chem. B* **1997**, *101*, 458.

Table 5. UV−Visible Spectral Parameters for TCHP and TPP Derivatives in CH_2Cl_2

	λ_{max} (nm)				
compound	Soret	visible			
H_2(TCHP)	422	525	562	603	660
H_2(TPP)	417	515	552	594	650
Zn(TCHP)	423	562	623		
Zn(TPP)	419	548	589		
Ni(TCHP)	426	550	587		
Ni(TPP)	414	525	557		

smaller for the TCHP derivatives than for the TPP ones, reflecting a larger destabilization of the HOMO compared to LUMO.

The same conclusion is obtained from electronic absorption spectra of the different neutral compounds. The UV−visible bands of the TCHP derivatives are red-shifted compared to those of the corresponding TPP complexes (Table 5). The lowest energy band in the visible region gives an indication of the HOMO−LUMO gap and indicates that the energy gap is smaller in the case of the tetracyclohexylporphyrins. The electronic effect due to the electron-donating cyclohexyl groups usually destabilizes both the HOMO and the LUMO. In contrast, a macrocycle distortion resulting from introduction of bulky groups should increase the energy of only the HOMO, without affecting the LUMO energy, and the consequence of this destabilization should result in a decrease of the HOMO−LUMO energy gap. This is what is observed by both the electrochemistry and the UV−visible spectroscopy, which suggests that macrocycle distortion in solution is more important in the case of the TCHP derivatives than in the case of the TPP porphyrins.

Conclusion

Substitution by cyclohexyl groups on the *meso* positions of a metalloporphyrin has notable stereochemical and electronic consequences. Steric crowding at the porphyrin periphery can be seen to be a quite complex issue. It results in a nonplanar distortion of the core, and the distortion type depends on the size of the metal ion. In the nickel complex Ni(TCHP), ruffling of the core leads to the shortest values observed for the $Ni-N_P$ distances. In contrast, the related zinc derivative Zn(TCHP) has a stepped core conformation to alleviate the crowding, and the $Zn-N_P$ distances are only slightly shorter than normal. Rotation of the cyclohexyl groups is fast on the NMR time scale at room temperature, and a 4-fold pseudosymmetry is observed by averaging of the signals of the four possible conformers. The more stable ($-g,g,-g,g$) conformer is prevalent at low temperatures in solutions of Zn(TCHP) and Ni(TCHP). In the two complexes, the porphyrin ring is easier to oxidize and harder to reduce than in their tetraphenylporphyrin congeners, in agreement with the stronger electron-donating effect of the cyclohexyl group.

Acknowledgment. We thank the CNRS (grant URA-1194 to J.C.M.), the NIH (grants GM-38401 and R.R.-06709 to W.R.S.), and the Robert A. Welch Foundation (grant E-680 to K.M.K.) for funding, and Dr. Michel Bardet for helpful discussions.

Supporting Information Available: Table S1, complete crystallographic details for Zn(TCHP) and Ni(TCHP); Table S2, atomic coordinates; Table S3, anisotropic displacement parameters; Table S4, atomic coordinates and isotropic displacement parameters for the fixed atoms; Table S5, bond lengths; Table S6, bond angles for [Ni(TCHP)·$CHCl_3$·CH_3CN]; Table S7, atomic coordinates; Table S8, anisotropic displacement parameters; Table S9, atomic coordinates and isotropic displacement parameters for the fixed atoms; Table S10, bond lengths; Table S11, bond angles for [Zn(TCHP)]; Figures S12 and S13, formal diagrams of the porphinato cores of Ni(TCHP) and Zn(TCHP) showing the patterns of displacements of atoms from the least-squares 24-atom plane in units of 0.01 Å. This material is available free of charge via the Internet at http://pubs.acs.org.

IC981233I